



HAL
open science

”Manipulation” of Crystal Structure by Methylthiolation Enabling Ultrahigh Mobility in a Pyrene-Based Molecular Semiconductor

Kazuo Takimiya, Kirill Bulgarevich, Mamatimin Abbas, Shingo Horiuchi,
Takuya Ogaki, Kohsuke Kawabata, Abduleziz Ablat

► **To cite this version:**

Kazuo Takimiya, Kirill Bulgarevich, Mamatimin Abbas, Shingo Horiuchi, Takuya Ogaki, et al.. ”Manipulation” of Crystal Structure by Methylthiolation Enabling Ultrahigh Mobility in a Pyrene-Based Molecular Semiconductor. *Advanced Materials*, 2021, 33 (32), pp.2102914. 10.1002/adma.202102914 . hal-03277911

HAL Id: hal-03277911

<https://hal.science/hal-03277911>

Submitted on 13 Jul 2021

HAL is a multi-disciplinary open access archive for the deposit and dissemination of scientific research documents, whether they are published or not. The documents may come from teaching and research institutions in France or abroad, or from public or private research centers.

L’archive ouverte pluridisciplinaire **HAL**, est destinée au dépôt et à la diffusion de documents scientifiques de niveau recherche, publiés ou non, émanant des établissements d’enseignement et de recherche français ou étrangers, des laboratoires publics ou privés.

Public Domain

“Manipulation” of Crystal Structure by Methylthiolation Enabling Ultrahigh Mobility in a Pyrene-Based Molecular Semiconductor

Kazuo Takimiya,* Kirill Bulgarevich, Mamatimin Abbas, Shingo Horiuchi, Takuya Ogaki, Kohsuke Kawabata, and Abduleziz Ablat

Control and prediction of crystal structures of molecular semiconductors are considered challenging, yet they are crucial for rational design of superior molecular semiconductors. It is here reported that through methylthiolation, one can rationally control the crystal structure of pyrene derivatives as molecular semiconductors; 1,6-bis(methylthio)pyrene keeps a similar sandwich herringbone structure to that of parent pyrene, whereas 1,3,6,8-tetrakis(methylthio)pyrene (MT-pyrene) takes a new type of brickwork structure. Such changes in these crystal structures are explained by the alteration of intermolecular interactions that are efficiently controlled by methylthiolation. Single crystals of MT-pyrene are evaluated as the active semiconducting material in single-crystal field-effect transistors (SC-FETs), which show extremely high mobility ($32 \text{ cm}^2 \text{ V}^{-1} \text{ s}^{-1}$ on average) operating at the drain and gate voltages of -5 V . Moreover, the band-like transport and very low trap density are experimentally confirmed for the MT-pyrene SC-FETs, testifying that the MT-pyrene is among the best molecular semiconductors for the SC-FET devices.

theoretical calculations at the molecular level are indeed indispensable tools in the design of new molecular semiconductors. In sharp contrast, prediction and control of the crystal structure of a given molecular semiconductor are difficult challenges to overcome.^[4] For this reason, molecular semiconductors have been developed by just considering the predictable molecular properties and/or by mimicking the molecular structures of already-known superior semiconducting molecules.

Historically, pentacene^[5] and one of its derivatives, 6,13-bis((triisopropylsilyl)ethynyl)pentacene (TIPS-pentacene) (Figure 1),^[6,7] have been the most important molecular semiconductors primarily because of the high carrier mobilities ($>1 \text{ cm}^2 \text{ V}^{-1} \text{ s}^{-1}$) of their field-effect transistors (FETs). Furthermore, their crystal

structures represent two prototypes of high-performance molecular semiconductors; although both are said to afford 2D electronic structures in the solid state,^[8] their crystal structures are significantly different from each other. Pentacene crystallizes into the herringbone structure,^[9] whereas TIPS-pentacene into the brickwork structure (often called a 2D π -stack structure).^[6] In contrast to the herringbone structure, which is a very common one for acenes^[10] and heteroacenes,^[11] the latter, brickwork structure, has been observed only in well-designed molecular semiconductors, where the mutual balance between the sizes of the bulky (trialkylsilyl)ethynyl substituent and π -core is

1. Introduction

Carrier transport in molecular semiconductors is governed by the electronic structure of the molecular solid, which is dictated by both the molecular properties (the energy levels and geometry of frontier molecular orbitals, molecular shapes, etc.) and crystal structure of molecular semiconductors.^[1] Thus, both of them must be considered to develop superior molecular semiconductors.^[2] Prediction and simulation of molecular properties by theoretical calculations, e.g., with Gaussian program packages,^[3] are now routinely carried out with considerable accuracy, and nowadays such

Prof. K. Takimiya, Dr. K. Bulgarevich, S. Horiuchi, Dr. T. Ogaki, Dr. K. Kawabata
RIKEN Center for Emergent Matter Science (CEMS)
2-1 Hirosawa, Wako, Saitama 351-0198, Japan
E-mail: takimiya@riken.jp

Prof. K. Takimiya, S. Horiuchi, Dr. K. Kawabata
Department of Chemistry
Graduate School of Science
Tohoku University
6-3 Aoba, Aramaki, Aoba-ku, Sendai, Miyagi 980-8578, Japan
Prof. K. Takimiya
Advanced Institute for Materials Research (WPI-AIMR)
Tohoku University
2-1-1 Katahira, Aoba-ku, Sendai, Miyagi 980-8577, Japan
Dr. M. Abbas, Dr. A. Ablat
IMS
University of Bordeaux
CNRS
UMR-5218
Bordeaux INP
ENSCBP
Talence 33405, France

 The ORCID identification number(s) for the author(s) of this article can be found under <https://doi.org/10.1002/adma.202102914>.

© 2021 The Authors. Advanced Materials published by Wiley-VCH GmbH. This is an open access article under the terms of the Creative Commons Attribution-NonCommercial-NoDerivs License, which permits use and distribution in any medium, provided the original work is properly cited, the use is non-commercial and no modifications or adaptations are made.

DOI: 10.1002/adma.202102914

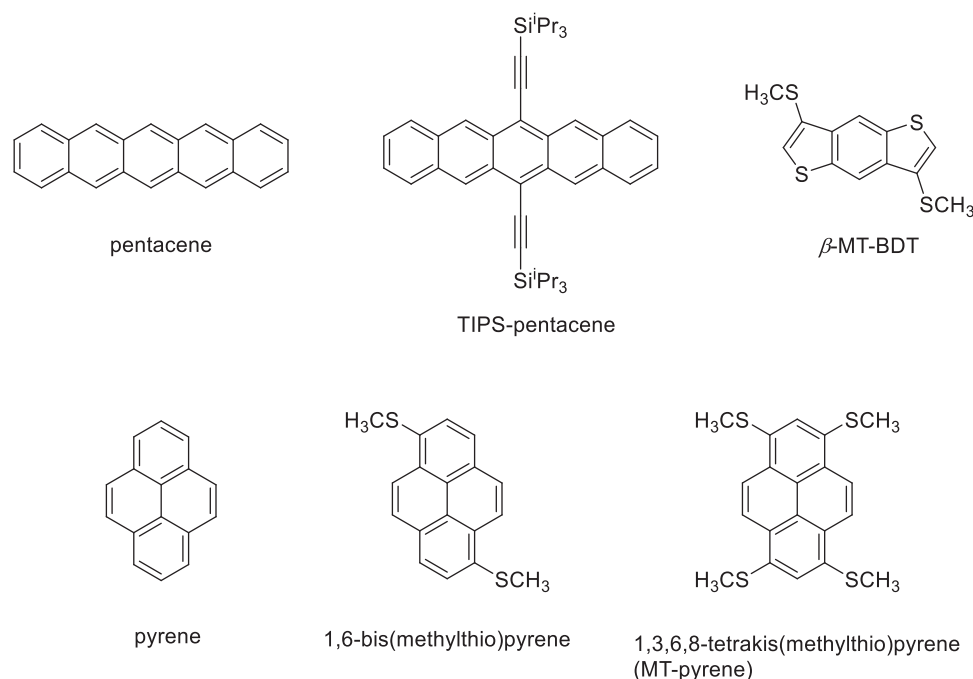


Figure 1. Structures of molecular semiconductors discussed in the present work.

tuned.^[12] With this strategy, a number of TIPS-pentacene-like acenes and heteroacenes have been synthesized,^[12b,13] and some of them have afforded high-performance FETs, which clearly testifies that the brickwork structure is a promising crystal structure for developing superior molecular semiconductors.

Despite such a successful example for the packing-structure control, i.e., the “TIPS-pentacene approach,” prediction, and/or control of crystal structures of molecular semiconductors by molecular design have still been limited.^[14] This is due to the lack of rational way to control intermolecular interaction in the molecular solid. Recently, we have found that methylthiolation at the β -position of thiophene rings of benzo[1,2-*b*:4,5-*b'*]dithiophene (β -MT-BDT, Figure 1) selectively changes the crystal structure from the herringbone in the parent compound to the rubrene-like pitched π -stack structure,^[15] that is, another promising crystal structure for high carrier mobility.^[16] The subsequent research on related molecular semiconductors, such as benzo[1,2-*b*:4,5-*b'*]diselenophene and naphtho-/anthra-[2,3-*b*:6,7-*b'*]dithiophenes, has demonstrated that the β -methylthiolation always induces structural change into the rubrene-like pitched π -stack,^[17] and the resulting molecular semiconductors afforded high-mobility FETs. All these structural changes in the solid state can be rationalized by the alteration of intermolecular interaction caused by the methylthio groups. In other words, methylthiolation at particular positions in π -conjugated systems could be a simple but potential way to control crystal structures of molecular semiconductors.

With these results, we propose that the control of crystal structures by methylthiolation will be a novel approach to realize superior molecular semiconductors. To embody this, we choose pyrene as the parent system, as its largely π -extended molecular structure can have potential to bring effective orbital overlap through face-to-face molecular aggregation in the solid state,^[18] though only limited pyrene derivatives known to date have shown decent carrier transport properties.^[19] The target

molecule in this study, 1,3,6,8-tetrakis(methylthio)pyrene (MT-pyrene, Figure 1), first reported in 1991,^[20] has turned out to crystallize into a new type of brickwork structure. We describe here the characteristic crystal structure of MT-pyrene caused by methylthiolation and the carrier transport properties elucidated by single-crystal FETs (SC-FETs).

2. Results

2.1. Crystal Structure of MT-Pyrene

MT-pyrene synthesized according to the reported procedure was carefully purified by multiple vacuum sublimation.^[20] Long and thin plates of MT-pyrene single crystals were obtained by physical vapor transport.^[21] The crystal structure of MT-pyrene shown in **Figure 2** is strikingly different from that of parent pyrene, which is known as the sandwich (or dimeric) herringbone structure,^[22] where a pair of pyrene molecules form a π -stacking dimer that packs into a herringbone-like motif (vide infra). In sharp contrast, MT-pyrene forms π -stacking structures both in the crystallographic [1 0 0] and [1 1 0] directions, which makes the MT-pyrene packing a new kind of brickwork structure (Figure 2a),^[23] reminiscent of the crystal structure of TIPS-pentacene. MT-pyrene forms a lamella structure along the crystallographic *c*-axis direction (Figure 2b), and, as a result, the crystallographic *ab* plane parallel to the substrate can act as the semiconducting channel in SC-FETs (vide infra).

The electronic structures of the semiconducting channel in the MT-pyrene crystal were examined by the theoretical calculations of intermolecular electronic coupling (or transfer integrals, t).^[24] The semiconducting channel in MT-pyrene consists of three kinds of molecular aggregates, i.e., two face-to-face aggregates ([1 0 0] and [1 1 0] directions, purple and cyan

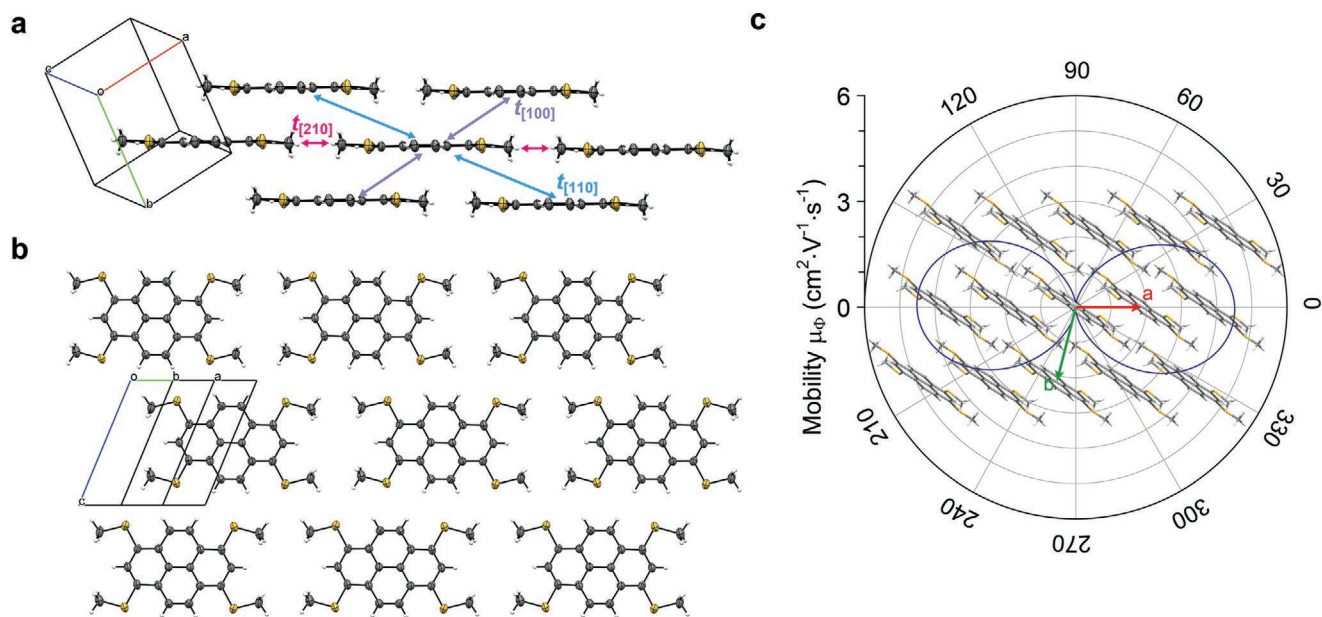


Figure 2. Crystal structure and simulated mobility of MT-pyrene single crystal. a) Crystal structure projected from the molecular short-axis direction with calculated orbital overlap of highest occupied molecular orbital (HOMO) and lowest unoccupied molecular orbital (LUMO); $t_{[100]} = 115.0$ meV (112.0) (purple), $t_{[110]} = 43.6$ meV (33.9) (cyan), and $t_{[210]} = 3.0$ (0.78) meV (magenta), respectively; note that the purple, cyan, and magenta arrows correspond to the crystallographic $[100]$, $[110]$, and $[210]$ directions. b) Molecular arrangement of MT-pyrene viewed along the normal to the molecular planes. c) Simulated anisotropic hole mobility calculated according to the hopping model.

arrows, respectively) and one end-to-end aggregate ($[210]$ direction, magenta arrow) (Figure 2a). Calculated t values for hole are 115.0 meV ($t_{[100]}$), 43.6 meV ($t_{[110]}$), and 3.0 meV ($t_{[210]}$), respectively, and those for electron are 112.0 meV ($t_{[100]}$), 33.9 meV ($t_{[110]}$), and 0.78 meV ($t_{[210]}$), respectively. The values of t s in the π -stack are larger than those reported in TIPS-pentacene and its related molecules (Figure S1, Supporting Information), and, in particular, one of the face-to-face aggregates, the $[100]$ direction, affords t s for both hole and electron greater than 100 meV. As the t s are not equivalent in the two face-to-face aggregates, MT-pyrene is not an ideal 2D electronic-structure system (Figure 2c),^[24] but the large absolute value of t s implies that MT-pyrene is promising as the active material in FET devices. In fact, the simulated hole mobility according to the hopping model exceeds $4.5 \text{ cm}^2 \text{ V}^{-1} \text{ s}^{-1}$ along the crystallographic a -axis direction (Figure 2c), implying the potential of MT-pyrene as a superior molecular semiconductor.

2.2. SC-FETs of MT-Pyrene

Free-standing long and thin plates of MT-pyrene grown by physical vapor transport (about 50–150 nm thick; Figure S2, Supporting Information) were laminated onto the Si/SiO₂ substrate with a 200 nm thick SiO₂ dielectric layer passivated with a CYTOP layer (CYTOP is a trademark of AGC Chemicals Company). The amorphous nature of CYTOP layers is known to prevent trap site formation at the active layer/gate dielectric interface typical for self-assembled monolayers (SAMs) such as octadecyltrichlorosilane (ODTS).^[25,26] This results in improved operational stability and smaller hysteresis in field-effect transistors (FETs). The source and drain electrodes were defined by

painting colloidal graphite (Figure 3a) or by sequential vapor deposition of molybdenum oxide (MoO₃) and gold through a shadow mask on top of the crystals (Figure S3a, Supporting Information). The X-ray diffraction (XRD) pattern of the crystals laminated on the substrates indicated that the crystallographic c -axis is along the normal to the substrate (Figure S4, Supporting Information). The channel direction, i.e., the longest direction of the plates, was determined to be the crystallographic a -axis direction by orientation analysis in the single-crystal XRD experiments, which corresponds to the direction of the largest transfer integral for hole (Figure 2a; Figure S5, Supporting Information).

The MT-pyrene-based SC-FETs showed clear p-channel behaviors under ambient condition (Figure 3b,c), which is consistent with the small ionization potential (5.2 eV) of the MT-pyrene single crystals evaluated by photoemission spectroscopy in air (Figure S6, Supporting Information). The devices showed textbook-like transistor behaviors; clear saturation at $V_d = -5$ V in the output characteristics (Figure 3b) and steep turn on with a small subthreshold slope (SS) of 120–150 mV dec⁻¹ (Figure 3c), the latter of which implies that the interface between the substrate and crystals has very low trap density (vide infra). Furthermore, the linear onset behaviors at the low V_d region in the output characteristics indicate negligible contact resistance of the device (Figure 3b). The mobility extracted from the saturation regime ($V_d = -5$ V, $V_g \geq -5$ V) is higher than $30 \text{ cm}^2 \text{ V}^{-1} \text{ s}^{-1}$ ($32 \text{ cm}^2 \text{ V}^{-1} \text{ s}^{-1}$ on average) with I_{on}/I_{off} being greater than 10^7 (Figure 3d), and the device performances are highly reproducible, which was confirmed by 26 devices fabricated on different crystals (Figure 3e). We also fabricated SC-FETs with different device architectures, e.g., top-contact devices with colloidal-graphite electrodes fabricated on an

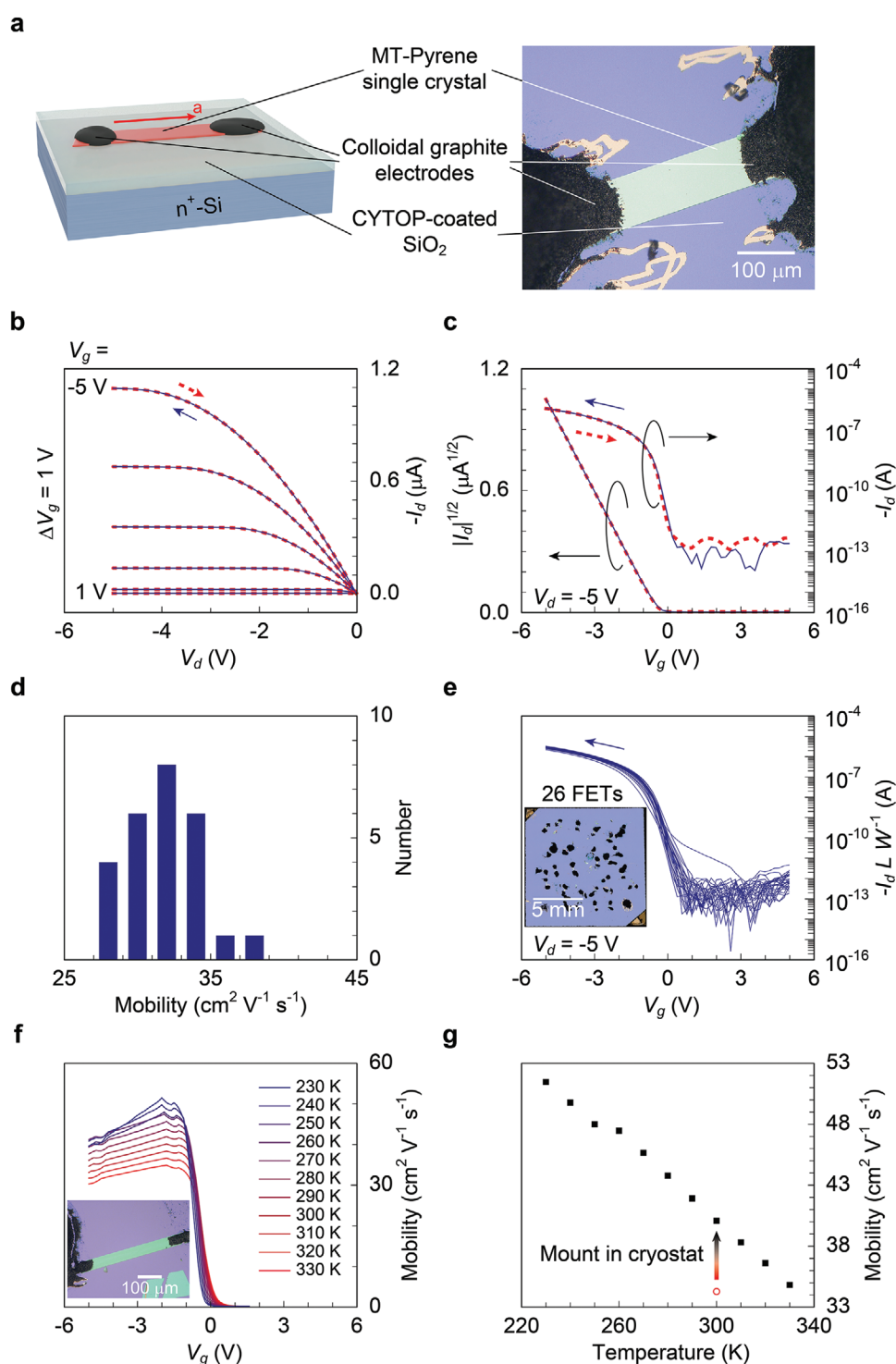


Figure 3. Characteristics of single-crystal field-effect transistors of MT-pyrene. a) Schematic device structure and optical microscopy image. b) Output characteristics. c) Transfer characteristics. d) Performance statistics from 26 devices. e) Transfer curves of 26 devices. L and W represent the channel length and width, respectively, of each individual FET. The inset is the optical microscopy image of the 26 devices. f) Gate-voltage-dependent mobilities from 330 to 230 K. The inset is the optical microscopy image of the SC-FET used in the low-temperature measurements. g) Temperature-dependent mobility (filled squares) at a maximum $|I_d|^{1/2}$ slope of 0.4 V_g interval of MT-pyrene SC-FET. The open circle indicates the mobility calculated from the initial transfer characteristics of the FET measured under ambient conditions before mounting in the cryostat.

ODTS SAM-modified Si/SiO₂ (Figure S3b, Supporting Information) and bottom-contact devices with the gold source and drain electrodes modified with pentafluorobenzenethiol (Figure S3c,

Supporting Information). These devices behaved similarly to those of the top-contact devices on the CYTOP passivation layer with a slightly decreased mobility (18–24 cm² V⁻¹ s⁻¹ on

average; Table S1, Supporting Information). These mobilities are among the highest for FETs with the active layer that consists of the brickwork crystal structure. It is thus safe to say that MT-pyrene is a promising high-mobility p-channel molecular semiconductor.

The experimental mobilities are much higher than those simulated according to the hopping model (Figure 2c), which strongly implies that the carrier transport observed for the MT-pyrene SC-FETs is band-like. To confirm this, temperature dependence of mobility was evaluated from 330 to 230 K. As clearly seen in Figure 3f,g, the mobility increases with the decrease of the temperature, which strongly supports the band-like transport in the MT-pyrene-based SC-FETs. At around 250 K, a tiny but abrupt anomaly in the mobility–temperature relationship was always observed in the measurements (Figure 3g). Similar anomaly of mobility in the low-temperature measurements was reported for the polymer-based FETs, which could be caused by residual water in the channel.^[27] However, we attribute the phenomenon to degradation of the graphite source/drain contacts since the mobility was not fully recovered in the heating process after the anomaly in the cooling process (Figure S7, Supporting Information). Causes for the contact degradation are not clear, but we speculate that the large thermal expansion coefficient of MT-pyrene crystal, which is estimated to be about $1.3 \times 10^{-4} \text{ K}^{-1}$ from the low-temperature single-crystal X-ray analyses (Table S3, Supporting Information), may relate to the phenomenon. In fact, the top-contact

devices with the MoO₃/Au source–drain electrodes showed slightly better temperature-dependence behavior, and the band-like transport was maintained down to 220 K (Figure S7, Supporting Information). When heating and cooling cycles were run above 250 K, the FETs fully recover the mobilities at high temperatures, confirming that the band-like transport that we observed comes purely from temperature variation.

3. Discussion

As mentioned above, the introduction of two methylthio groups on benzo[1,2-*b*:4,5-*b'*]dithiophene and its related compounds reproducibly induces structural change from the herringbone to the pitched π -stack. In this structural change, the methylthio groups play critical roles, that is, to disrupt the CH– π intermolecular interaction between the π -face and the peri-hydrogen atoms at the edge of the molecule in the parent systems and to bring about the CH– π intermolecular interaction between the π -face and the hydrogen atoms at thiophene α -position and the methyl moiety, together with the face-to-face π -stacking.^[17a] Intriguingly, the crystal structure of 1,6-bis(methylthio)pyrene recently reported by Wang et al. is classified into a sandwich herringbone structure similar to that of parent pyrene.^[28] We thus analyze in detail the intermolecular interaction in the crystal structures of parent pyrene, 1,6-bis(methylthio)pyrene (Figure 4), and MT-pyrene (Figure 5; Table S2, Supporting

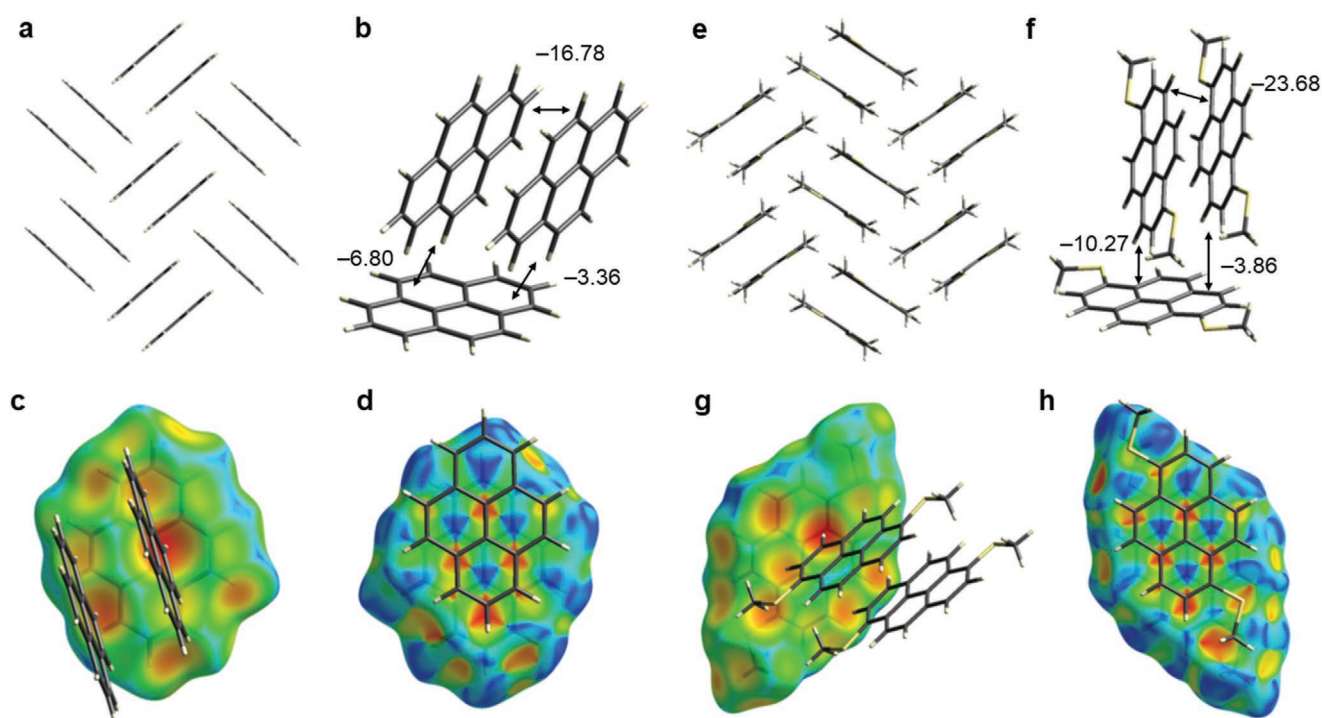


Figure 4. Crystal structures of parent pyrene and 1,6-bis(methylthio)pyrene. a) Sandwich herringbone structure of parent pyrene. b) Intermolecular interaction energies (kcal mol^{-1}) calculated by SAPT analysis for parent pyrene. c) Hirshfeld surface analysis mapped with d_e (distance from the Hirshfeld surface to the nearest nucleus outside of the surface) for the edge-to-face aggregates observed in the parent pyrene, in which the red depression spots on the Hirshfeld surface represent the intermolecular CH– π contacts. d) Hirshfeld surface analysis mapped with shape index, in which the pair of red and blue triangles represent π – π interaction in the stacking dimer of parent pyrene. e) Sandwich herringbone structure of 1,6-bis(methylthio)pyrene. f) Intermolecular interaction energies (kcal mol^{-1}) for 1,6-bis(methylthio)pyrene. g) Hirshfeld surface analysis mapped with d_e for the edge-to-face aggregates observed in 1,6-bis(methylthio)pyrene. h) Hirshfeld surface analysis mapped with shape index in the stacking dimer of 1,6-bis(methylthio)pyrene.

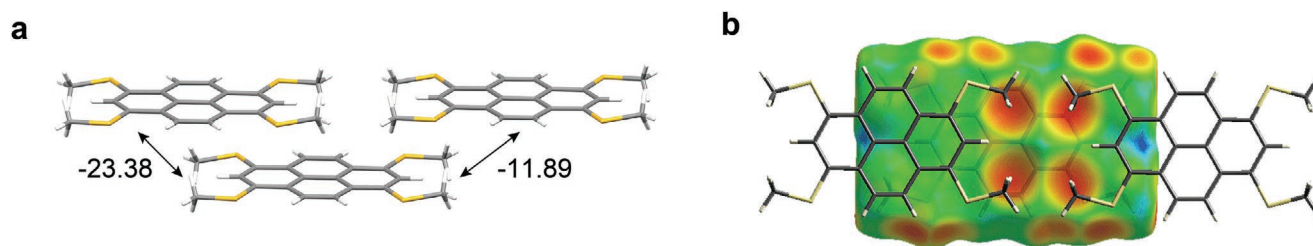


Figure 5. Crystal structures of MT-pyrene. a) Intermolecular interaction energies (kcal mol^{-1}) calculated by the SAPT method. b) Hirshfeld surface mapped with d_e (distance from the Hirshfeld surface to the nearest nucleus outside of the surface) of MT-pyrene.

Information). The inspection revealed that the former two have similar features in intermolecular interactions; there exist two types of molecular aggregates, namely, the face-to-face (π -stacking) and the edge-to-face ($\text{CH}-\pi$) aggregates. These aggregates contribute to the stabilization of the crystal structure of pyrene (-16.78 and -6.80 kcal mol^{-1}) and 1,6-bis(methylthio)pyrene (-23.68 and -0.27 kcal mol^{-1}), respectively, mainly by dispersion force, according to the theoretical calculations of intermolecular forces by symmetry-adapted perturbation theory (SAPT) method with jun-cc-pvdz level using the PSI4 program package (Table S2, Supporting Information).^[29] In addition, the Hirshfeld surface analysis shows that intermolecular contacts between the large π -faces can be responsible for the stabilization of the face-to-face aggregate, whereas the intermolecular contacts between the hydrogen atoms and π -face of the neighboring molecule in the edge-to-face aggregate (Figure 4) also contribute to the stabilization. The two methylthio groups in 1,6-bis(methylthio)pyrene do not disrupt the edge-to-face aggregation completely, owing to remaining two sets of hydrogen arrays (3-, 4-positions and 8-, 9-positions) that can serve to form the intermolecular $\text{CH}-\pi$ contacts (Figure 4f,g).

In contrast, four methylthio groups at the 1-, 3-, 6-, and 8-positions in MT-pyrene make the hydrogen atoms for the intermolecular $\text{CH}-\pi$ contacts observed in the parent and 1,6-bis(methylthio)pyrene unavailable, thus disabling the formation of edge-to-face aggregate. On the other hand, the face-to-face aggregates are maintained, where the molecules largely slip along the molecular long axis, probably owing to the intermolecular repulsion between the methylthio groups. As a result, two types of face-to-face aggregates are observed. The SAPT calculations demonstrate that these face-to-face aggregates are largely stabilized energetically (-23.38 and -11.89 kcal mol^{-1} , respectively) (Figure 5a). Interestingly, the Hirshfeld surface of MT-pyrene mapped with d_e shows four red depression parts beneath the methyl groups of neighboring molecules, implying that the methylthio groups contribute to energetically stabilize the face-to-face aggregates through the dispersion forces (Figure 5b).^[30]

These analyses on the crystal structures of pyrene and its methylthiolated derivatives highlight the critical roles of the methylthio groups; first, four methylthio groups disrupt the edge-to-face interaction in the parent system and then induce the attractive interaction to stabilize two types of face-to-face aggregates, resulting in a new kind of brickwork structure. Second, two methylthio groups at the 1- and 6-positions are not sufficient to induce such a drastic structural change in the pyrene system, indicative of the importance of completely

disrupting the existing intermolecular interaction in the parent system to induce the structural change.

The MT-pyrene-based SC-FETs can be characterized by the high mobility and low operational voltages. The band-like transport confirmed by the temperature dependence of mobility could rationalize the high mobility. Band calculations reveal the electronic structure of MT-pyrene molecular solid, which features large HOMO bandwidths in the $\Gamma-X$ (≈ 481 meV) and $\Gamma-V$ (432 meV) directions, and small effective masses (m^*) of ≈ 0.58 ($\Gamma-X$) and 1.05 ($\Gamma-V$), respectively (Figure S8, Supporting Information). This also indicates that the anisotropy of mobility should not be that large as the one estimated by the hopping model (Figure 2c). To confirm this, the SC-FETs with the channel direction almost perpendicular to the long crystal axis (crystallographic a -axis) were fabricated, and the devices showed a mobility of about 9 $\text{cm}^2 \text{V}^{-1} \text{s}^{-1}$ (Figure S9, Supporting Information), which is almost the one third of the value evaluated along the long crystal axis.

Furthermore, to understand the capability of low-voltage operation, we estimate the trap density of interface between the MT-pyrene crystal and substrate surface from subthreshold slope, SS.^[31] A trap density of $1.3 \times 10^{11} \text{ cm}^{-2}$ calculated for the SC-FETs fabricated on CYTOP-passivated Si/SiO₂ substrate is comparable with those of the best pentacene-^[31] and rubrene-SC-FETs.^[32] The very low trap density could be related to very flat surface of the MT-pyrene crystals (Figure S2, Supporting Information).

Overall, MT-pyrene can be regarded as an excellent, new class of molecular semiconductors that compete against the best molecular semiconductors for SC-FETs so far reported,^[33] e.g., rubrene,^[34] C₈-BTBT,^[35,36] and C₁₀-DNBDT.^[37] It is interesting to point out that the methyl moieties exist in the MT-pyrene semiconducting layer; involvement of sp³ carbon atoms that do not contribute to intermolecular π -orbital overlap is quite unusual for such superior molecular semiconductors. This implies that more flexible molecular design than ever could be possible to develop novel molecular semiconductors.

4. Conclusion

We have demonstrated the possibility of crystal-structure control by methylthiolation on pyrene from the sandwich herringbone in parent pyrene to the brickwork structure in MT-pyrene. The theoretical calculations assist to understand the structural change in the series of methylthiolated pyrene derivatives, i.e., the number and position of the group are the key to control

the crystal structure. The resulting brickwork structure of MT-pyrene affords very large orbital overlap (>100 meV) and functions as an excellent FET channel showing a very high hole mobility of $32 \text{ cm}^2 \text{ V}^{-1} \text{ s}^{-1}$ in the SC-FET devices operated at $V_d = V_g = -5 \text{ V}$. The MT-pyrene SC-FETs are thus characterized by high mobility and low-voltage operation; the former is explained by the band-like transport confirmed by temperature dependence of mobility as well as the band calculations demonstrating the large bandwidth and small effective mass. On the other hand, the low trap density in the MT-pyrene SC-FETs estimated from the subthreshold properties rationalizes the latter. All these excellent device characteristics compare well with those of the best organic SC-FETs so far reported. This means that MT-pyrene, which is easily synthesized in only two steps from parent pyrene, is an excellent molecular semiconductor. In addition, the bottom-up approach, i.e., the crystal-structure control by the molecular design, is a promising way to develop novel excellent molecular semiconductors, and further investigation according to this is now underway in our group.

5. Experimental Section

Synthesis and Preparation of Single Crystals of MT-Pyrene: MT-pyrene was synthesized from 1,3,6,8-tetrabromopyrene and sodium methanethiolate according to the reported procedure.^[20] The crude product including a trace amount of 1-bromo-3,6,8-tris(methylthio)pyrene was treated with lithium aluminum hydride in tetrahydrofuran (THF) to convert the impurity to 1,3,6-tris(methylthio)pyrene, which was easily removed by sublimation, and the resulting product was purified by multiple train sublimation under vacuum. With the purified powder sample, single crystals were grown by the physical vapor transport technique under a flow of nitrogen carrier gas. Based on the thermogravimetric analysis (Figure S10, Supporting Information), the temperatures of the source and crystallization zone were set to 240 and 130 °C, respectively, as measured using thermolabels (NiCK).

X-ray Structural Analysis: Single-crystal X-ray analysis of MT-pyrene was carried out with relatively thick crystals (1–10 μm) obtained by the PVT technique on a Rigaku Oxford Diffraction XtaLAB Synergy Custom DW system with a HyPix-6000HE detector (Cu Kα radiation, wavelength: 1.5418 Å, multilayer confocal optics). The structures were solved by the SHELXT program.^[38] Non-hydrogen atoms were refined anisotropically.^[39] All calculations were carried out by using the crystallographic software package Olex2 (version 1.3.0).^[40] Crystal data: orange plate, “triclinic,” $P\bar{1}$, $a = 6.5536(7)$, $b = 7.9935(14)$, $c = 9.3715(10)$ Å, $\alpha = 111.132(13)$, $\beta = 101.623(10)$, $\gamma = 98.940(11)^\circ$, $V = 434.34(11)$ Å³, $Z = 2$, $T = 293(2)$ K, $R = 0.0916$, $wR^2 = 0.2498$, goodness of fit (GOF) = 1.083. The crystal structure of MT-pyrene was also solved under different temperatures (Table S3, Supporting Information). X-ray diffractions of laminated crystals of MT-pyrene on the substrates were recorded on a Rigaku Ultima IV with a Cu Kα radiation (wavelength: 1.54184 Å).

Fabrication of SC-FETs: Heavily doped n-type Si wafers with thermally grown SiO₂ layers were used as substrates. The substrates were cleaned by sonication in acetone for 10 min two times followed by ultraviolet-ozone treatment for more than 30 min. The substrates were spin-coated with 3 wt% CYTOP (AGC) solution at 3000 rpm for 1 min, and then dried at 180 °C on a hot plate in air. The thickness of the CYTOP film (≈90 nm) was measured using atomic force microscopy (AFM, NanoNavi IIs/NanoCute). For the bottom-contact FETs, the Au source and drain electrodes (50 nm) were deposited directly on the CYTOP film by physical vapor deposition under $<5 \times 10^{-4}$ Pa. The modification of Au electrodes with pentafluorobenzenethiol (PFBT, purchased from TCI Chemicals) was performed by immersion in 50×10^{-3} M solution in ethanol for more than 8 h under ambient conditions.^[41] The MT-pyrene crystals grown by the physical vapor transport method were carefully

transferred from the glass substrates to the top of the CYTOP film using a tungsten needle or a nylon loop. The top-contact FETs were completed by placing the droplets of colloidal graphite (source and drain electrodes) on each side of the crystal and drying for more than 30 min under ambient conditions. Alternatively, vapor deposition of MoO₃/Au top electrodes was performed as follows. A metal shadow mask was carefully positioned on the laminated crystal to cover the middle part of the crystal. MoO₃ layer (15 nm thick) was deposited at a rate of $<0.3 \text{ Å s}^{-1}$ under $<5 \times 10^{-4}$ Pa. The vacuum chamber was opened, and the sample position was adjusted to minimize the mismatch between the MoO₃ and Au layers. Finally, the Au layer (30 nm thick) was deposited at a rate of $<0.5 \text{ Å s}^{-1}$ under $<5 \times 10^{-4}$ Pa. All the FET measurements were performed with a probe station and a semiconductor parameter analyzer (Keithley 4200-SCS) in air. The carrier mobility, μ , was determined from the forward swing of the transfer characteristics using Equation (1)

$$|I_d| = \frac{W}{2L} C_i \mu (V_g - V_{th})^2 \quad (1)$$

where L and W are channel length and width of the FETs, respectively, C_i is the gate capacitance per unit area, and V_{th} is the threshold voltage. C_i was determined to be 8.6 nF cm^{-2} by using a $2.5 \times 1.5 \text{ mm}^2$ Au electrode deposited on the CYTOP surface (8.8 nF cm^{-2} for the substrates used in low-temperature measurements). Low-temperature measurements were carried out in the liquid nitrogen cryostat system. Additional silver paste was used to connect the graphite (or MoO₃/Au) contacts to the copper wires. Several transfer curves were taken at each temperature until a stable curve was obtained.

Note that all the device characteristics were maintained during more than 130 days under ambient conditions (Figure S11, Supporting Information).

Theoretical Calculations: The geometries of isolated molecules in the neutral and cationic states were optimized using the B3LYP/6–31g(d) level with Gaussian 16 program package.^[3] The reorganization energy (λ) of the molecules was calculated by using the adiabatic potential energy surface method in Equation (2)

$$\lambda = \lambda_0 + \lambda_+ = (E_0^* - E_0) + (E_+^* - E_+) \quad (2)$$

where E_0^* , E_0 , E_+^* , and E_+ represent the energies of a neutral molecule in the cationic geometry, a neutral molecule in the optimized geometry, a cationic molecule in the neutral geometry, and a cationic molecule in the optimized geometry, respectively.^[24] Intermolecular electronic coupling (transfer integral, t) in different molecular dimers extracted from the single-crystal structures was calculated with the Amsterdam Density Functional (ADF) program.^[42] With λ_s and t_s , anisotropic theoretical mobilities were calculated according to the reported procedure.^[24] Intermolecular interaction energies for dimers of pyrene, 1,6-bis(methylthio)pyrene and MT-pyrene extracted from the crystal structures were calculated by SAPT calculations with jun-cc-pvdz level using the PSI4 program package. Hirshfeld surfaces were computed on CrystalExplore 17.5 program to visualize intermolecular contacts in the crystalline state.^[43] Band structure calculations were carried out with Quantum Espresso program^[44] employing a plane-wave basis set, the Perdew–Burke–Ernzerhof (PBE) functional,^[45] and projector augmented wave (PAW) pseudopotentials,^[46] and using $12 \times 12 \times 1$ k -point Pack–Monkhorst net with the geometry determined by the single-crystal X-ray analysis. The carrier effective masses were evaluated by parabolic fitting at the band extrema (I – X and I – V directions).^[47]

[CCDC 2076078–2076087 contains the crystallographic data for this paper. These data can be obtained free of charge from The Cambridge Crystallographic Data Centre via www.ccdc.cam.ac.uk/data_request/cif]

Supporting Information

Supporting Information is available from the Wiley Online Library or from the author.

Acknowledgements

The authors gratefully acknowledge the Supercomputer System in the Advanced Center for Computing and Communication (ACCC) of RIKEN for support in theoretical calculations. The authors also thank the Center for Computational Materials Science, Institute for Materials Research, Tohoku University for the use of MASAMUNE-IMR (Materials science Supercomputing system for Advanced Multi-scale simulations towards NExt-generation-Institute for Materials Research). This work was financially supported by JSPS KAKENHI (Grant Nos. JP19H00906, JP20K22421, and JP20H05865) and the Mitsubishi Foundation. The authors also thank the Bilateral Programs between Japan and France supported by JSPS and CNRS. A.A. acknowledges the financial support of the French government PAUSE program.

Conflict of Interest

The authors declare no conflict of interest.

Data Availability Statement

The data that support the findings of this study are available from the corresponding author upon reasonable request.

Keywords

band-like transport, crystal structure, organic semiconductor, single-crystal field-effect transistor, ultrahigh mobility

Received: April 17, 2021

Revised: May 14, 2021

Published online:

- [1] a) V. Coropceanu, J. Cornil, D. A. da Silva Filho, Y. Olivier, R. Silbey, J.-L. Brédas, *Chem. Rev.* **2007**, *107*, 926; b) J. E. Anthony, *Angew. Chem., Int. Ed.* **2008**, *47*, 452; c) K. Takimiya, S. Shinamura, I. Osaka, E. Miyazaki, *Adv. Mater.* **2011**, *23*, 4347.
- [2] K. Takimiya, M. Nakano, H. Sugino, I. Osaka, *Synth. Met.* **2016**, *217*, 68.
- [3] M. J. Frisch, G. W. Trucks, H. B. Schlegel, G. E. Scuseria, M. A. Robb, J. R. Cheeseman, G. Scalmani, V. Barone, G. A. Petersson, H. Nakatsuji, X. Li, M. Caricato, A. V. Marenich, J. Bloino, B. G. Janesko, R. Gomperts, B. Mennucci, H. P. Hratchian, J. V. Ortiz, A. F. Izmaylov, J. L. Sonnenberg, D. Williams-Youngs, F. Ding, F. Lipparini, F. Egidi, J. Goings, B. Peng, A. Petrone, T. Henderson, D. Ranasinghe, V. G. Zakrzewski, J. Gao, N. Rega, G. Zheng, W. Liang, M. Hada, M. Ehara, K. Toyota, R. Fukuda, J. Hasegawa, M. Ishida, T. Nakajima, Y. Honda, O. Kitao, H. Nakai, T. Vreven, K. Throssell, J. A. Montgomery Jr., J. E. Peralta, F. Ogliaro, M. J. Bearpark, J. J. Heyd, E. N. Brothers, K. N. Kudin, V. N. Staroverov, T. A. Keith, R. Kobayashi, J. Normand, K. Raghavachari, A. P. Rendell, J. C. Burant, S. S. Iyengar, J. Tomasi, M. Cossi, J. M. Millam, M. Klene, C. Adamo, R. Cammi, J. W. Ochterski, R. L. Martin, K. Morokuma, O. Farkas, J. B. Foresman, D. J. Fox, *Gaussian 16 Rev. C.01*, Gaussian, Inc., Wallingford, CT, USA **2016**.
- [4] a) S. L. Price, *Chem. Soc. Rev.* **2014**, *43*, 2098; b) A. M. Reilly, R. I. Cooper, C. S. Adjiman, S. Bhattacharya, A. D. Boese, J. G. Brandenburg, P. J. Bygrave, R. Bylisma, J. E. Campbell, R. Car, D. H. Case, R. Chadha, J. C. Cole, K. Cosburn, H. M. Cuppen, F. Curtis, G. M. Day, R. A. DiStasio Jr., A. Dzyabchenko, B. P. van Eijck, D. M. Elking, J. A. van den Ende, J. C. Facelli, M. B. Ferraro, L. Fusti-Molnar, C.-A. Gatsiou, T. S. Gee, R. de Gelder, L. M. Ghiringhelli, H. Goto, S. Grimme, R. Guo, D. W. M. Hofmann, J. Hoja, R. K. Hylton, L. Iuzzolino, W. Jankiewicz, D. T. de Jong, J. Kendrick, N. J. J. de Klerk, H.-Y. Ko, L. N. Kuleshova, X. Li, S. Lohani, F. J. J. Leusen, A. M. Lund, J. Lv, Y. Ma, N. Marom, A. E. Masunov, P. McCabe, D. P. McMahon, H. Meekes, M. P. Metz, A. J. Misquitta, S. Mohamed, B. Monserrat, R. J. Needs, M. A. Neumann, J. Nyman, S. Obata, H. Oberhofer, A. R. Oganov, A. M. Orendt, G. I. Pagola, C. C. Pantelides, C. J. Pickard, R. Podeszwa, L. S. Price, S. L. Price, A. Pulido, M. G. Read, K. Reuter, E. Schneider, C. Schober, G. P. Shields, P. Singh, I. J. Sugden, K. Szalewicz, C. R. Taylor, A. Tkatchenko, M. E. Tuckerman, F. Vacarro, M. Vasileiadis, A. Vazquez-Mayagoitia, L. Vogt, Y. Wang, R. E. Watson, G. A. de Wijs, J. Yang, Q. Zhu, C. R. Groom, *Acta Crystallogr., Sect. B: Struct. Sci., Cryst. Eng. Mater.* **2016**, *72*, 439.
- [5] a) D. J. Gundlach, Y. Y. Lin, T. N. Jackson, S. F. Nelson, D. G. Schlom, *IEEE Electron Device Lett.* **1997**, *18*, 87; b) Y. Lin, D. J. Gundlach, S. F. Nelson, T. N. Jackson, *IEEE Electron Device Lett.* **1997**, *18*, 606.
- [6] J. E. Anthony, J. S. Brooks, D. L. Eaton, S. R. Parkin, *J. Am. Chem. Soc.* **2001**, *123*, 9482.
- [7] C. D. Sheraw, T. N. Jackson, D. L. Eaton, J. E. Anthony, *Adv. Mater.* **2003**, *15*, 2009.
- [8] a) G. A. de Wijs, C. C. Mattheus, R. A. de Groot, T. T. M. Palstra, *Synth. Met.* **2003**, *139*, 109; b) O. Ostroverkhova, D. G. Cooke, F. A. Hegmann, R. R. Tykwinski, S. R. Parkin, J. E. Anthony, *Appl. Phys. Lett.* **2006**, *89*, 192113.
- [9] R. B. Campbell, J. M. Robertson, J. Trotter, *Acta Crystallogr.* **1962**, *15*, 289.
- [10] M. Watanabe, Y. J. Chang, S.-W. Liu, T.-H. Chao, K. Goto, M. M. Islam, C.-H. Yuan, Y.-T. Tao, T. Shinmyozu, T. J. Chow, *Nat. Chem.* **2012**, *4*, 574.
- [11] K. Takimiya, I. Osaka, T. Mori, M. Nakano, *Acc. Chem. Res.* **2014**, *47*, 1493.
- [12] a) J. E. Anthony, D. L. Eaton, S. R. Parkin, *Org. Lett.* **2002**, *4*, 15; b) J. E. Anthony, *Chem. Rev.* **2006**, *106*, 5028.
- [13] a) M. M. Payne, S. R. Parkin, J. E. Anthony, C.-C. Kuo, T. N. Jackson, *J. Am. Chem. Soc.* **2005**, *127*, 4986; b) S. Subramanian, S. K. Park, S. R. Parkin, V. Podzorov, T. N. Jackson, J. E. Anthony, *J. Am. Chem. Soc.* **2008**, *130*, 2706; c) Q. Miao, *Adv. Mater.* **2014**, *26*, 5541; d) U. H. F. Bunz, *Acc. Chem. Res.* **2015**, *48*, 1676; e) M. Chu, J.-X. Fan, S. Yang, D. Liu, C. F. Ng, H. Dong, A.-M. Ren, Q. Miao, *Adv. Mater.* **2018**, *30*, 1803467; f) A. J. Petty, Q. Ai, J. C. Sorli, H. F. Haneef, G. E. Purdum, A. Boehm, D. B. Granger, K. Gu, C. P. L. Rubinger, S. R. Parkin, K. R. Graham, O. D. Jurchescu, Y.-L. Loo, C. Risko, J. E. Anthony, *Chem. Sci.* **2019**, *10*, 10543.
- [14] Z.-F. Yao, J.-Y. Wang, J. Pei, *Cryst. Growth Des.* **2018**, *18*, 7.
- [15] C. Wang, H. Nakamura, H. Sugino, K. Takimiya, *Chem. Commun.* **2017**, *53*, 9594.
- [16] a) V. Podzorov, E. Menard, A. Borissov, V. Kiryukhin, J. A. Rogers, M. E. Gershenson, *Phys. Rev. Lett.* **2004**, *93*, 086602; b) M. D. Curtis, J. Cao, J. W. Kampf, *J. Am. Chem. Soc.* **2004**, *126*, 4318.
- [17] a) H. Takenaka, T. Ogaki, C. Wang, K. Kawabata, K. Takimiya, *Chem. Mater.* **2019**, *31*, 6696; b) C. Wang, D. Hashizume, M. Nakano, T. Ogaki, H. Takenaka, K. Kawabata, K. Takimiya, *Chem. Sci.* **2020**, *11*, 1573.
- [18] a) T. M. Figueira-Duarte, K. Müllen, *Chem. Rev.* **2011**, *111*, 7260; b) Y. Gong, X. Zhan, Q. Li, Z. Li, *Sci. China: Chem.* **2016**, *59*, 1623.
- [19] H. Cho, S. Lee, N. S. Cho, G. E. Jabbour, J. Kwak, D.-H. Hwang, C. Lee, *ACS Appl. Mater. Interfaces* **2013**, *5*, 3855.
- [20] G. Heywang, S. Roth, *Angew. Chem., Int. Ed. Engl.* **1991**, *30*, 176.
- [21] R. A. Laudise, C. Kloc, P. G. Simpkins, T. Siegrist, *J. Cryst. Growth* **1998**, *187*, 449.
- [22] A. Camerman, J. Trotter, *Acta Crystallogr.* **1965**, *18*, 636.

- [23] T. Nakazato, W. Matsuda, T. Sakurai, S. Seki, H. Shinokubo, Y. Miyake, *Chem. Lett.* **2020**, 49, 465.
- [24] S.-H. Wen, A. Li, J. Song, W.-Q. Deng, K.-L. Han, W. A. Goddard, *J. Phys. Chem. B* **2009**, 113, 8813.
- [25] W. L. Kalb, T. Mathis, S. Haas, A. F. Stassen, B. Batlogg, *Appl. Phys. Lett.* **2007**, 90, 092104.
- [26] K. Bulgarevich, K. Sakamoto, T. Yasuda, T. Minari, M. Takeuchi, *Adv. Electron. Mater.* **2020**, 6, 2000161.
- [27] a) H. L. Gomes, P. Stallinga, M. Cölle, D. M. de Leeuw, F. Biscarini, *Appl. Phys. Lett.* **2006**, 88, 082101; b) M. Kemerink, T. Hallam, M. J. Lee, N. Zhao, M. Caironi, H. Siringhaus, *Phys. Rev. B* **2009**, 80, 082101.
- [28] G.-Q. Wang, H.-B. Fang, L.-H. Xu, Z.-H. Ni, *Z. Kristallogr. - New Cryst. Struct.* **2019**, 234, 929.
- [29] a) B. Jeziorski, R. Moszynski, K. Szalewicz, *Chem. Rev.* **1994**, 94, 1887; b) R. M. Parrish, L. A. Burns, D. G. A. Smith, A. C. Simmonett, A. E. DePrince, E. G. Hohenstein, U. Bozkaya, A. Y. Sokolov, R. Di Remigio, R. M. Richard, J. F. Gonthier, A. M. James, H. R. McAlexander, A. Kumar, M. Saitow, X. Wang, B. P. Pritchard, P. Verma, H. F. Schaefer, K. Patkowski, R. A. King, E. F. Valeev, F. A. Evangelista, J. M. Turney, T. D. Crawford, C. D. Sherrill, *J. Chem. Theory Comput.* **2017**, 13, 3185.
- [30] K. Takimiya, T. Ogaki, C. Wang, K. Kawabata, *Chem. - Asian J.* **2020**, 15, 915.
- [31] W. L. Kalb, B. Batlogg, *Phys. Rev. B* **2010**, 81, 035327.
- [32] C. Goldmann, C. Krellner, K. P. Pernstich, S. Haas, D. J. Gundlach, B. Batlogg, *J. Appl. Phys.* **2006**, 99, 034507.
- [33] X. Zhang, H. Dong, W. Hu, *Adv. Mater.* **2018**, 30, 1801048.
- [34] V. C. Sundar, J. Zaumseil, V. Podzorov, E. Menard, R. L. Willett, T. Someya, M. E. Gershenson, J. A. Rogers, *Science* **2004**, 303, 1644.
- [35] H. Minemawari, T. Yamada, H. Matsui, J. y. Tsutsumi, S. Haas, R. Chiba, R. Kumai, T. Hasegawa, *Nature* **2011**, 475, 364.
- [36] C. Liu, T. Minari, X. Lu, A. Kumatani, K. Takimiya, K. Tsukagoshi, *Adv. Mater.* **2011**, 23, 523.
- [37] C. Mitsui, T. Okamoto, M. Yamagishi, J. Tsurumi, K. Yoshimoto, K. Nakahara, J. Soeda, Y. Hirose, H. Sato, A. Yamano, T. Uemura, J. Takeya, *Adv. Mater.* **2014**, 26, 4546.
- [38] G. Sheldrick, *Acta Crystallogr., Sect. A: Found. Adv.* **2015**, 71, 3.
- [39] G. Sheldrick, *Acta Crystallogr., Sect. C: Struct. Chem.* **2015**, 71, 3.
- [40] O. V. Dolomanov, L. J. Bourhis, R. J. Gildea, J. A. K. Howard, H. Puschmann, *J. Appl. Crystallogr.* **2009**, 42, 339.
- [41] T. Nagase, S. Abe, T. Kobayashi, Y. Kimura, A. Hamaguchi, Y. Ikeda, H. Naito, *J. Phys.: Conf. Ser.* **2017**, 924, 012008.
- [42] Amsterdam Density Functional (ADF): powerful DFT code for modeling molecules; Software for Chemistry & Materials BV, Amsterdam, The Netherlands; <https://www.scm.com/ADF/>.
- [43] a) J. J. McKinnon, M. A. Spackman, A. S. Mitchell, *Acta Crystallogr., Sect. B: Struct. Sci., Cryst. Eng. Mater.* **2004**, 60, 627; b) M. J. Turner, J. J. McKinnon, S. K. Wolff, D. J. Grimwood, M. A. Spackman, D. Jayatilaka, M. A. Spackman, *CrystalExplorer17*; University of Western Australia, 2017; <http://hirshfeldsurface.net>.
- [44] P. Giannozzi, S. Baroni, N. Bonini, M. Calandra, R. Car, C. Cavazzoni, D. Ceresoli, G. L. Chiarotti, M. Cococcioni, I. Dabo, A. Dal Corso, S. de Gironcoli, S. Fabris, G. Fratesi, R. Gebauer, U. Gerstmann, C. Gougoussis, A. Kokalj, M. Lazzeri, L. Martin-Samos, N. Marzari, F. Mauri, R. Mazzarello, S. Paolini, A. Pasquarello, L. Paulatto, C. Sbraccia, S. Scandolo, G. Sclauzero, A. P. Seitsonen, A. Smogunov, P. Umari, R. M. Wentzcovitch, *J. Phys.: Condens. Matter* **2009**, 21, 395502.
- [45] J. P. Perdew, K. Burke, M. Ernzerhof, *Phys. Rev. Lett.* **1996**, 77, 3865.
- [46] P. E. Blöchl, *Phys. Rev. B* **1994**, 50, 17953.
- [47] M. Z. S. Flores, V. N. Freire, R. P. dos Santos, G. A. Farias, E. W. S. Caetano, M. C. F. de Oliveira, J. R. L. Fernandez, L. M. R. Scolfaro, M. J. B. Bezerra, T. M. Oliveira, G. A. Bezerra, B. S. Cavada, H. W. Leite Alves, *Phys. Rev. B* **2008**, 77, 115104.